Revised Soil Classification System for Coarse-Fine Mixtures

Junghee Park[1] and J. Carlos Santamarina, A.M.ASCE[2]

Abstract: Soil classification systems worldwide capture great physical insight and enable geotechnical engineers to anticipate the properties and behavior of soils by grouping them into similar response categories based on their index properties. Yet gravimetric analysis and data trends summarized from published papers reveal critical limitations in soil group boundaries adopted in current systems. In particular, current classification systems fail to capture the dominant role of fines on the mechanical and hydraulic properties of soils. A revised soil classification system (RSCS) for coarse-fine mixtures is proposed herein. Definitions of classification boundaries use low and high void ratios that gravel, sand, and fines may attain. This research adopts $e^{\max}$ and $e^{\min}$ for gravels and sands, and three distinctive void ratio values for fines: soft $e_F|^{10\ \mathrm{kPa}}$ and stiff $e_F|^{1\ \mathrm{MPa}}$ for mechanical response (at effective stress 10 kPa and 1 MPa, respectively), and viscous $\lambda \cdot e_F|^{\mathrm{LL}}$ for fluid flow control, where $\lambda = 2\log(\mathrm{LL} - 25)$ and $e_F|^{\mathrm{LL}}$ is the void ratio at the liquid limit. For classification purposes, these void ratios can be estimated from index properties such as particle shape, the coefficient of uniformity, and the liquid limit. Analytically computed and data-adjusted boundaries are soil-specific, in contrast with the Unified Soil Classification System (USCS). Threshold fractions for mechanical control and for flow control are quite distinct in the proposed system. Therefore, the RSCS uses a two-name nomenclature whereby the first letters identify the component(s) that controls mechanical properties, followed by a letter (shown in parenthesis) that identifies the component that controls fluid flow. Sample charts in this paper and a Microsoft *Excel* facilitate the implementation of this revised classification system. **DOI: 10.1061/(ASCE)GT.1943-5606.0001705.**

Author keywords: Textural chart; Soil properties; Unified Soil Classification System.

Introduction

Soil classification enables geotechnical engineers to anticipate the properties and behavior of soils by grouping them into similar response categories based on their index properties (Casagrande 1948; Howard 1984; Das 2009; Dundulis et al. 2010; Kovačević and Jurić-Kaćunić 2014).

The Unified Soil Classification System (ASTM 2011) is the foundation for classification systems worldwide, from Japan and China (Japanese Geotechnical Society 2009; Chinese Standard 2007) to Mexico and Switzerland (Association Suisse de Normalization 1959). The USCS places emphasis on particle size and uses the percentage retained on Sieve No. 200 (75 μm) to separate coarse-grained soils (more than 50% retained) from fine-grained soils (more than 50% passing). Other classification systems use a lower boundary for fines, either 35% (ASTM 2009; BSI 1999; SETRA and LCPC 2000; and Australia's guidelines under review) or 40% (Deutche Norm 2011).

Most classification systems, including the USCS, use a 50% split on Sieve No. 4 (4.76 mm) to classify coarse-grained soils as either gravels or sands. The German DIN 18196 classifies soils as gravel when the fraction coarser than 2 mm exceeds 40%.

A detailed analysis of the USCS and other soil classification systems highlighted previously readily discloses great physical insight and understanding of soil behavior and their properties. However, both laboratory and field data gathered during the last century indicate the need for a revised soil classification system (RSCS). There are common limitations to all classification systems. First, they adopt fixed boundaries for coarse-fine mixtures despite the fact that fine-grained soils may exhibit a broad range of plasticity. Second, particle shape and grading affect the packing density of the coarse fraction, and hence the relevance of both the coefficients of uniformity and curvature in the USCS, yet shape does not feature in any classification system. Third, the effect of plastic fines on mechanical and conduction properties is not properly captured by the 50% and the 5–12% fines thresholds adopted in the USCS. Finally, current soil classification systems do not reflect the fact that pore-fluid chemistry plays a significant role in the behavior of fines.

The purpose of this study is to propose a RSCS for engineering purposes by providing a physics-inspired, data-driven approach that benefits from the experience gained since the inception of current soil classification systems. This study starts with gravimetric-volumetric analyses to anticipate fines and sand fraction thresholds, summarizes a data-based analysis focused on the physical properties of soil mixtures, and concludes with a new methodology for soil classification.

Granular Mixtures: Triangular Textural Charts

A soil can be analyzed as a three-component mixture made of gravel, sand, and fines. Triangular textural charts then facilitate the grouping of similar soils [Fig. 1(a) for interpretation guidelines]. Fig. 1(b) depicts the essence of the USCS in such a triangular chart. This soil map does not capture additional classification details

[1]Ph.D. Student, Earth Science and Engineering, King Abdullah Univ. of Science and Technology, Building 5, Thuwal 23955-6900, Saudi Arabia (corresponding author). E-mail: junghee.park@kaust.edu.sa

[2]Professor, Earth Science and Engineering, King Abdullah Univ. of Science and Technology, Building 5, Thuwal 23955-6900, Saudi Arabia.

Note. This manuscript was submitted on July 5, 2016; approved on January 12, 2017; published online on April 17, 2017. Discussion period open until September 17, 2017; separate discussions must be submitted for individual papers. This paper is part of the ***Journal of Geotechnical and Geoenvironmental Engineering***, © ASCE, ISSN 1090-0241.

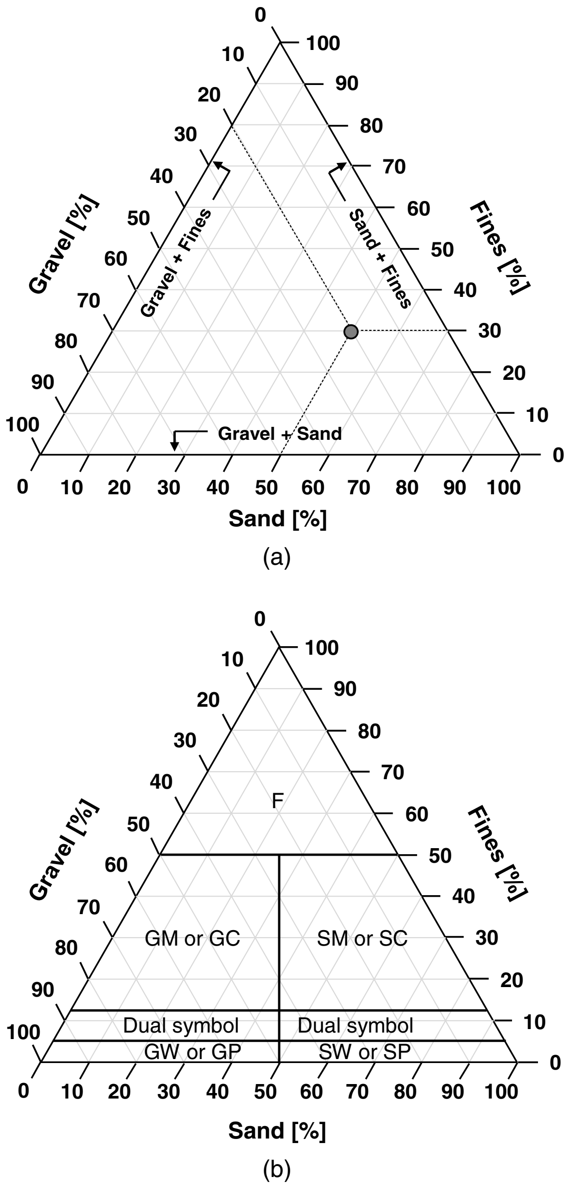

Fig. 1. Soil classification systems: (a) guide for the interpretation of triangular gravel-sand-fines charts; the example corresponds to gravel fraction $F_G = 20\%$, sand fraction $F_S = 50\%$, and fines fraction $F_F = 30\%$; (b) the USCS

related to the coefficients of uniformity and curvature for coarse grains and Atterberg limits for fine grains.

The gravimetric-volumetric analysis of mixtures allows for the systematic definition of threshold boundaries in these triangular charts. The simpler case of binary mixtures is presented first.

Binary Mixtures

Invoke gravimetric-volumetric relations to compute the mass fraction of fines F_F in coarse-fine mixtures when fine grains completely fill the voids between coarse grains (Fig. 2). In terms of the void ratio of fines e_F and coarse e_C fractions, and assuming the same specific gravities (see Appendix for the detailed mathematical solution)

$$F_F = \frac{M_F}{M_T} = \frac{M_F}{M_C + M_F} \approx \frac{e_C}{1 + e_C + e_F} \quad \text{and} \quad F_C = 1 - F_F \tag{1}$$

There are two threshold fines fractions (Fig. 2). Densely packed coarse grains filled with loosely packed fine grains define the low threshold fines fraction $F_F|^L$. By contrast, loosely packed coarse grains filled with densely packed fine grains result in the high threshold fines fraction $F_F|^H$.

The low- and high-threshold fines fractions divide binary mixtures into three groups (Fig. 2): coarse-dominant $F_F < F_F|^L$, transitional $F_F|^L < F_F < F_F|^H$, and fines-dominant $F_F > F_F|^H$ mixtures. This analysis applies to binary gravel-sand, gravel-fines, and sand-fines mixtures.

Threshold Ternary Mixtures: Gravel-Sand-Fines Mixtures

Extend the previous gravimetric-volumetric analysis to ternary gravel-sand-fines mixtures. In this case, sand packed at void ratio e_S fills the voids in the gravel e_G, and fines e_F fill the remaining pores within the gravel-sand mixture. Then the computed gravel fraction F_G, sand fraction F_S, and fines fraction F_F are functions of their void ratios (Appendix details the complete mathematical solution)

$$F_G = \frac{1}{\left(1 + \frac{e_G}{1+e_S} + \frac{e_S}{1+e_F}\frac{e_G}{1+e_S}\right)} \tag{2}$$

$$F_S = \frac{1}{\left(\frac{1+e_S}{e_G} + 1 + \frac{e_S}{1+e_F}\right)} \tag{3}$$

$$F_F = \frac{1}{\left(\frac{1+e_S}{e_G}\frac{1+e_F}{e_S} + \frac{1+e_F}{e_S} + 1\right)} \tag{4}$$

where $F_G + F_S + F_F = 1.0$. The combination of loose and dense packing conditions for each component leads to various threshold fractions, similar to binary mixtures. These threshold values define a transitional zone in a triangular textural plot for ternary mixtures, rather than the line segment for binary mixtures shown in Fig. 2.

Low and High Void Ratios: Correlations

The use of gravimetric-volumetric analyses to determine transition thresholds require estimates of feasible low and high void ratios for gravel G, sand S, and fines F. Robust empirical relations between index properties and feasible void ratios can facilitate soil classification.

Gravel and Sand

Because packing densities for gravels and sands are insensitive to effective stress, the threshold fractions derived from the packing states of gravels and sands are independent of effective stress as a first approximation. The maximum and minimum void ratios e^{max} and e^{min} are adopted to estimate the feasible range of void ratios gravels and sands may attain (Fig. 2).

Maximum and minimum void ratios decrease for rounder and well-graded sands and gravels. Indeed, roundness R and uniformity C_u determine e^{max} and e^{min} (Youd 1973)

$$e_C^{max} = 0.032 + \frac{0.154}{R} + \frac{0.522}{C_u} \tag{5}$$

$$e_C^{min} = -0.012 + \frac{0.082}{R} + \frac{0.371}{C_u} \tag{6}$$

where roundness R is the average radius of curvature of surface features $\sum r_i/N$ divided by the radius of the largest inscribed

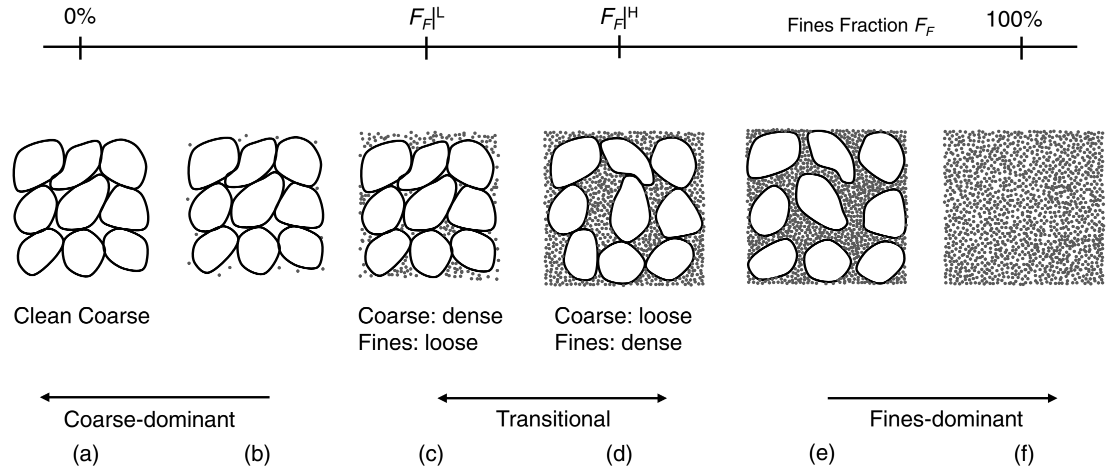

Fig. 2. Coarse-fine mixtures: threshold fractions; coarse-dominant, transitional, and fines-dominant mixtures; these conceptual sketches apply to gravel-sand, gravel-fines, and sand-fines mixtures

sphere $r_{\max}$. Readily available software computes grain roundness R from grain images; for classification purposes, it is sufficient to visually compare grains against shape charts [chart in Krumbein and Sloss (1963), example in Cho et al. (2006)]. Alternatively, the value of $e^{\max}$ can be quickly determined using a container of known volume and a scale, and $e^{\min} = 0.74[e^{\max} - 0.15(C_u - 1)]$ is an adequate estimate of $e^{\min}$ (Cho et al. 2006).

Fines

Load Carrying Criterion

The void ratio of fines (i.e., silts and clays) depends on their plasticity and the applied effective stress. Effective stress is not a soil index property, but is a state variable. One may argue against the use of a state variable in soil classification; however, a sand-clay mixture that behaves as clay-dominant at low effective stress may transform into sand-dominant at high effective stress as clays consolidate and sand grains form the load-carrying skeleton [a similar notion underlies the equivalent liquidity index in Schofield (1980)]. Consequently, the void ratio of fines at preselected effective stress levels are selected as equivalent index parameters that capture the packing condition of fines, analogous to the use of $e^{\max}$ and $e^{\min}$ for coarse grains.

The K_0-compression line at effective stress $\sigma' = 10$ kPa and $\sigma' = 1$ MPa defines two useful reference void ratios $e_F|^{10\ \mathrm{kPa}}$ and $e_F|^{1\ \mathrm{MPa}}$ that represent soft and stiff soil conditions relevant to near-surface engineering applications. Published correlations enable the prediction of reference void ratios in the absence of consolidation data during early soil classification (Burland 1990; Chong and Santamarina 2016)

$$e_F|^{10\ \mathrm{kPa}} = e_F|^{1\ \mathrm{kPa}} - C_c = 0.026\mathrm{LL} + 0.07 \tag{7}$$

$$e_F|^{1\ \mathrm{MPa}} = e_F|^{1\ \mathrm{kPa}} - 3C_c = 0.011\mathrm{LL} + 0.21 \tag{8}$$

These lower-bound estimates apply to nonsensitive clays or remolded conditions; they reflect that the void ratio at the liquid limit $e_F|^{\mathrm{LL}} = G_s\mathrm{LL}/100$ is a good estimator of the void ratio at $\sigma' = 1$ kPa because $e_F|^{1\ \mathrm{kPa}} \approx 5/4 e_F|^{\mathrm{LL}} = 0.033\mathrm{LL}$ (Chong and Santamarina 2016) and of the compressibility of fine-grained sediments $C_c = 0.007(\mathrm{LL} - 10)$ (Skempton and Jones 1944). For the proposed revised classification system, these estimates must use the liquid limit obtained for fines passing through Sieve No. 200 (75-μm opening).

Flow Control Criterion

The presence of fines has a prevalent role on hydraulic conductivity even when fines are packed at a void ratio higher than $e_F|^{\mathrm{LL}}$. In fact, fluid flow can exacerbate the effect of fines by dragging grains until they clog the soil by forming bridges at pore constrictions (Kenney and Lau 1985; Skempton and Brogan 1994; Valdes and Santamarina 2006, 2008; Shire et al. 2014).

In this context, the threshold fines fraction for fluid flow adopted in this classification is the fines content that causes a 100-fold decrease in the hydraulic conductivity of otherwise clean sands and clean gravels. Fines and water may form a viscous slurry at low fines content. Analyses based on published data (Locat and Demers 1988; Palomino and Santamarina 2005; Pennekamp et al. 2010) and experiments conducted as part of this study indicate that such a slurry will exhibit ~100 times higher viscosity than water when the water content is approximately $\omega\% = \lambda\mathrm{LL}$, where $\lambda = [2 \cdot \log(\mathrm{LL} - 25)] \geq 1.0$. Then, the void ratio of fines used to compute the threshold fines fraction for fluid flow $e_F|^{\mathrm{flow}}$ is

$$e_F|^{\mathrm{flow}} = \lambda\cdot e_F|^{\mathrm{LL}} = [2\log(\mathrm{LL} - 25)] \cdot e_F|^{\mathrm{LL}} \approx 0.05\mathrm{LL} \cdot \log(\mathrm{LL} - 25) \quad (\text{where } \lambda \geq 1) \tag{9}$$

where $e_F|^{\mathrm{LL}}$ = void ratio of fines at the liquid limit.

Data Collection: Transitions in Dominant Behavior

Gravimetric-volumetric analyses in terms of the low and high void ratios identified previously may not properly capture the transition from coarse-controlled to fines-controlled behavior because of multiple grain-scale and pore-scale mechanisms and processes.

This study gathered mixture properties from published studies to examine the transition in hydraulic conductivity, shear wave velocity, compression index, and shear strength. Table 1 presents each data set normalized between the properties for 100% coarse grains and 100% fines to facilitate the comparison across different soil types. In addition, an asymptotically consistent mixture model was selected to fit all trends. The normalization function and mixture models are mathematically analogous for all x-properties (Table 1)

Table 1. Property Normalization and Fitting Models

Trend with fines	Property	Normalization and fitting trend	Threshold fraction F_{th}: Coarse-fine (%)	Threshold fraction F_{th}: Gravel-sand (%)	Notes
Saddles	Porosity (n)	$n = n_c \cdot \{\exp[\sqrt{(F_i - F_{th})^2}]^a - b\}$	15–40	20–40	F_{th} decreases with increasing relative size ratio R_d
Increases	Compression index (C_c)	$\underline{\underline{C_c}} = \frac{C_{c,i} - C_{c,C}}{C_{c,F} - C_{c,C}} = 1 - \frac{\sqrt{1-F_i^6}}{1+\left(\frac{F_i}{F_{th}}\right)^m}$	10–65	No data	F_{th} increases with decreasing liquid limit of fines
Decreases	Hydraulic conductivity (k)	$\underline{\underline{k}} = \frac{k_i - k_F}{k_C - k_F} = \frac{\sqrt{1-F_i^6}}{1+\left(\frac{F_i}{F_{th}}\right)^m}$	2–7	5–17	F_{th} decreases with increasing relative size ratio R_d and angularity
	Shear wave velocity (V_s)	$\underline{\underline{V_s}} = \frac{V_{s,i} - V_{s,F}}{V_{s,C} - V_{s,F}} = \frac{\sqrt{1-F_i^6}}{1+\left(\frac{F_i}{F_{th}}\right)^m}$	7–36	No data	F_{th} increases with increasing relative size ratio R_d and increasing effective stress
	Shear strength ($\tan\phi$)	$\underline{\underline{\tan\phi}} = \frac{\tan\phi_i - \tan\phi_F}{\tan\phi_C - \tan\phi_F} = \frac{\sqrt{1-F_i^6}}{1+\left(\frac{F_i}{F_{th}}\right)^m}$	10–42	47–70	F_{th} decreases with increasing relative size ratio R_d and increasing fines plasticity

Note: Threshold fraction F_{th} is near the property arithmetic mean (except for porosity, where it is selected as the fines content at minimum porosity); subscripts G = gravel, S = sand, F = fines; model parameters are a, b, and m.

$$\frac{x_i - x_F}{x_C - x_F} = \frac{\sqrt{1-F_i^6}}{1+(\frac{F_i}{F_{th}})^m} \tag{10}$$

where x_i corresponds to a coarse-fine mixture with fines fraction F_i; and x_C and x_F = values of the property for 100% coarse and 100% fines fractions. The role of the numerator in the mixture model is to force the convergence of the normalized property to zero as $F_i \to 1$. The arithmetic mean $x_i = (x_C + x_F)/2$ takes place near the threshold fines fraction $F_i \approx F_{th}$. Table 1 illustrates mixture models fitted to the data to identify the threshold fractions F_{th} for all properties. The data set includes porosity to gain an insight into the underlying processes related to granular packing. Observations for each physical property follow.

Porosity

Fig. 3 illustrates the changes in porosity with fines fraction in coarse-fine mixtures and with sand fraction in gravel-sand mixtures. The minimum porosities are attained at $F_F = 15$–40% in coarse-fine mixtures, and at $F_S = 20$–40% in gravel-sand mixtures. In general, the porosity of mixtures decreases with increases in roundness (Youd 1973; Santamarina and Cho 2004; Cho et al. 2006), coefficient of uniformity C_u (Istomina 1957; Vukovic and Soro 1992), and relative size ratio R_d (McGeary 1961; Guyon et al. 1987; Marion et al. 1992; Thevanayagam 2007). Geometric models for idealized packings agree with these data-based observations (e.g., Koltermann and Gorelick 1995; Kamann et al. 2007).

Hydraulic Conductivity

Fig. 4 presents normalized hydraulic conductivity data $\underline{\underline{k}}$ versus fines F_F and sand F_S fractions. While hydraulic conductivity varies in orders of magnitude, linear normalization was chosen to reflect the direct proportionality between the flow rate q and hydraulic conductivity k in engineering problems, according to Darcy's law $q = kiA$ (i = hydraulic gradient, A = area). The hydraulic conductivity drops to the arithmetic mean value when the fines fraction is $F_F = 2$–7% in coarse-fine mixtures, and when the sand fraction is $F_S = 5$–17% in gravel-sand mixtures. While these threshold fractions arise from gap-graded mixture data, similar threshold values are expected for well-graded mixtures following the discussion on porosity trends in the previous section.

The data include mixtures with hydraulic conductivity smaller than the hydraulic conductivity of 100% fines in coarse-fine mixtures, or smaller than for 100% sand in gravel-sand mixtures (this is clearly observed in logarithmic scale, but it is faint in the normalized scale used in Fig. 4). Hydraulic conductivity values $k_{mix} < k_F$ reflect the increased tortuosity of flow paths caused by the presence of coarse grains floating in the porous medium made of the finer grains.

Small-Strain Stiffness in Terms of Shear Wave Velocity

Fig. 5 shows normalized shear wave velocities $\underline{\underline{V_s}}$, as defined in Table 1, for coarse-fine mixtures against fines fraction F_F. The normalized shear wave velocities drop to the arithmetic mean value for threshold fines fractions between $F_{th} = 5$ and 36%. The transition from coarse-controlled to fines-controlled shear stiffness is influenced by effective stresses: as the vertical effective stresses increases, the threshold fines fraction F_{th} increases. Apparently, fines prevent the formation of a coarse-grain skeleton at low stress but consolidate at high stress levels. Fig. 5(b) displays data for sand-mica mixtures in the absence of published data for gravel-sand mixtures. Results indicate that d_{sand}/L_{mica} affects the transition from coarse-controlled to fines-controlled mixtures, and the threshold fines fraction F_{th}.

Compression Index

Fig. 6 presents the normalized compression index $\underline{\underline{C_c}}$ of coarse-fine mixtures graphed versus fines fraction F_F. The normalized compression index reaches the arithmetic mean compressibility at a fines fraction that varies from $F_{th} = 10$–65% as the liquid limit decreases from high-plasticity clays to silts. The initial void ratio, particle shape, soil fabric, stress conditions, pore fluids, mineralogy, and plasticity of fines all affect the transition from coarse-controlled to fines-controlled compressibility (Kenney 1977; Maio and Fenellif 1994; Sridharan and Nagaraj 2000; Monkul and Ozden 2007; Thevanayagam 2007; Bandini and Sathiskumar 2009).

The threshold fines fraction for the sand-silt mixture is $F_{th} = 65$%, as illustrated by the open square in Fig. 6. Yet, mixtures

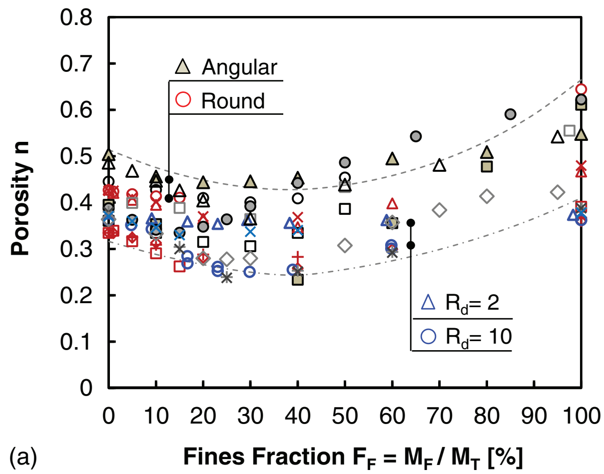

Data sources: ● Han et al. 1986; ○,△ Guyon et al. 1987; ■ Knoll and Knight 1994; × Zlatovic and Ishihara 1995; ◇ Yamamuro and Covert 2001; + Thevanayagam et al. 2002; □ Konishi et al. 2007; × Thevanayagam 2007; △ Yang 2004; □,○ Belkhatir et al. 2013; ○,△,×,◇,□ Choo 2013; ▲ Kang and Lee 2015 (Note that analogous data are found in Lade and Yamamuro 1997; Fourie and Papageorgiou 2001; Shafiee 2008).

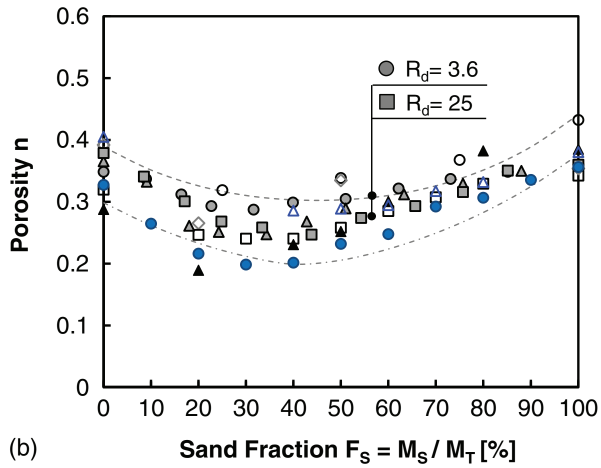

Data sources: ● Vallejo 2001; ○ Indrawan et al. 2006; △ Simoni and Houlsby 2006; ◇ Rahardjo et al. 2008; ▲, ■ Li 2009; ●,▲,■ Zhang and Ward 2011 (Note that analogous data are found in Kamann et al. 2007; Donohue 2008).

Fig. 3. (Color) Porosity: (a) coarse-fine mixtures; (b) gravel-sand mixtures; $R_d = D_{50}/d_{50}$ is the relative size ratio (D_{50} = median grain size of coarser grains; d_{50} = median grain size of finer grains); for model—plotted as dashed line—refer to Table 1

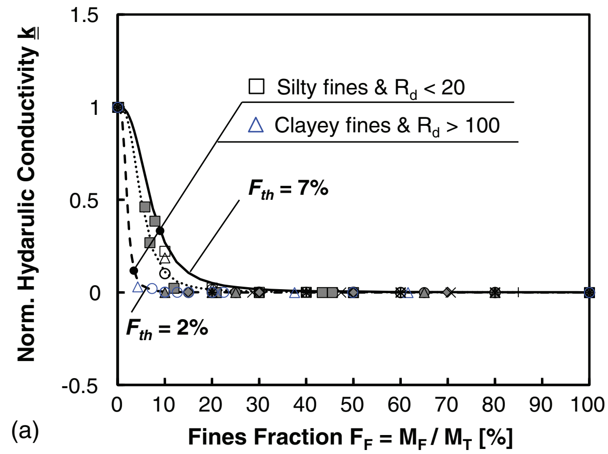

Data sources: ■ Marion 1990; ✶,+ Shelley and Daniel 1993; △ Knoll and Knight 1994; ▲, ● Sivapullaiah et al. 2000; ○ Crawford et al. 2008; × Shafiee 2008; ○ Tanaka and Toida 2008; ◆ Steiakakis et al. 2012; □,△ Belkhatir et al. 2013.

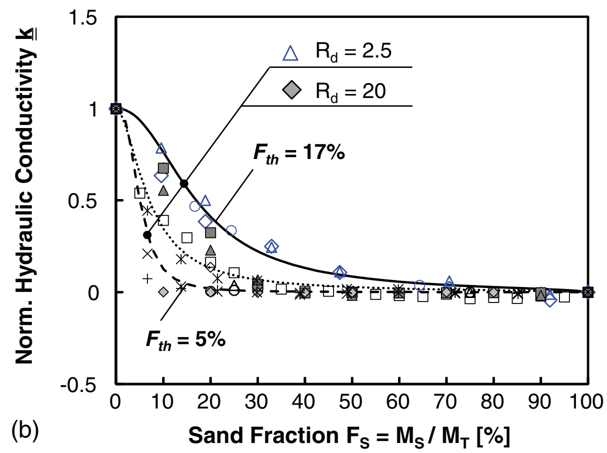

Data sources: ◇,■, ▲ Mason 1997; △,○ Indrawan et al. 2006; ○ Kamann et al. 2007; □ Donohue 2008; ● Rahardjo et al. 2008; ◆ Tanaka and Toida 2008; ×,✶,+ Zhang and Ward 2011; ◇,△ Lee and Koo 2014.

Fig. 4. (Color) Normalized hydraulic conductivity: (a) coarse-fine mixtures; (b) gravel-sand mixtures; $R_d = D_{50}/d_{50}$ is the relative size ratio (D_{50} = median grain size of coarser grains; d_{50} = median grain size of finer grains); Table 1 defines the normalization and the fitting model (plotted here as lines)

near the minimum porosity (i.e., at a fines fraction $F_F \approx 30\%$) exhibit lower compressibility than the 100% sand specimen (this effect is concealed in the normalized scale used in Fig. 6). Similarly, while coarse grains form a load-bearing skeleton when the fines fraction is lower than threshold values (Monkul and Ozden 2007; Evans and Valdes 2011), fines improve the stability of the soil matrix by hindering the buckling of the coarse-grain chains (Radjai et al. 1998; Lee et al. 2007a).

Shear Strength in Terms of tan ϕ

Fig. 7 presents trends for the normalized tan ϕ plotted against the fraction of fines and sand. The data in Fig. 7 were obtained by various researchers using different test devices, and include peak, constant volume, and residual friction angles. While diverse in origin, all trends show consistent transitions from coarse-controlled to fines-controlled shear strength. The threshold fraction characterizes the transition from coarse-controlled to fines-controlled shear strength. The fines threshold is $F_{th} = 10$–42% in coarse-fine mixtures while the sand threshold is $F_{th} = 47$–70% in gravel-sand mixtures. The threshold fraction F_{th} decreases when the relative size ratio R_d increases, the liquid limit increases, the coarse grains become well graded, and the particle shape becomes rounder. These trends reflect underlying changes in shear mechanisms, e.g., from rolling to sliding shear (Kenney 1967; Lupini et al. 1981; Maio and Fenellif 1994; Mitchell and Soga 2005; Santamarina and Shin 2009; Skempton 1985). The dominant mechanism depends on whether fines occupy the pores between coarse grains, or separate coarse grains apart (Monkul and Ozden 2007; Thevanayagam et al. 2002; Vallejo and Mawby 2000), and associated changes in the coordination number, rotational frustration, and interlocking (Santamarina et al. 2001; Bareither et al. 2008; Cho et al. 2006).

Particle shape rather than size determines the constant volume friction angle (Cho et al. 2006). Therefore, angular fines could exhibit higher friction angle than well-rounded coarser particles.

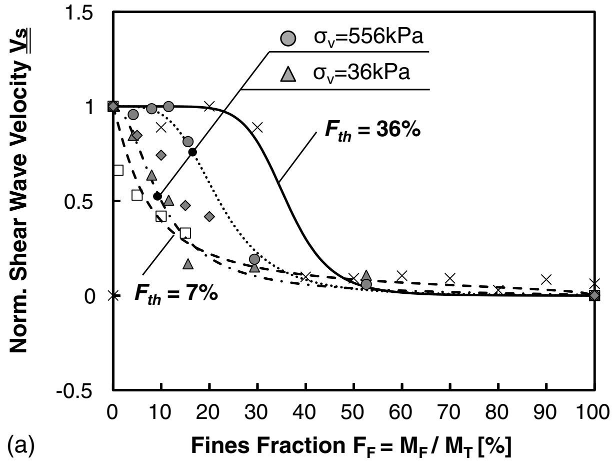

Data sources: ◆ Salgado et al. 2000; × Vallejo and Lobo-Guerrero 2005; ▲,● Lee et al. 2007a; □ Choo 2013 (*$V_{s,max}$ and $V_{s,min}$ are used for the normalization of symbol × only).

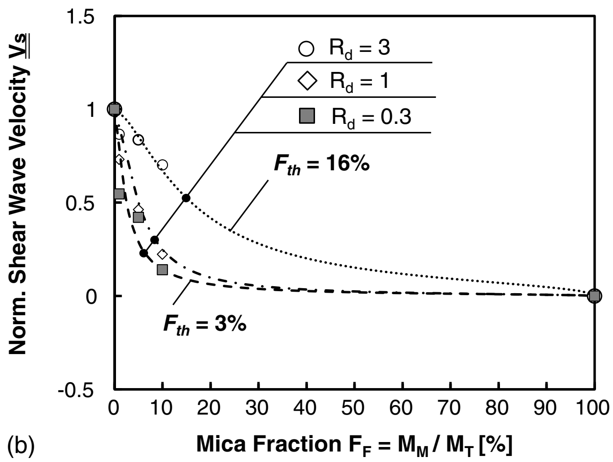

Data sources: ○,◇,■ Lee et al. 2007b.

Fig. 5. Normalized shear wave velocity: (a) coarse-fine mixtures; (b) sand-mica mixtures; $R_d = D_{50}/L_{\text{mica}}$ is the relative size ratio for sand-mica (D_{50} = median grain size of sand; L_{mica} = median mica particle length); F_{th} denotes the threshold mica fraction by weight; Table 1 defines the normalization and the fitting model (plotted here as lines)

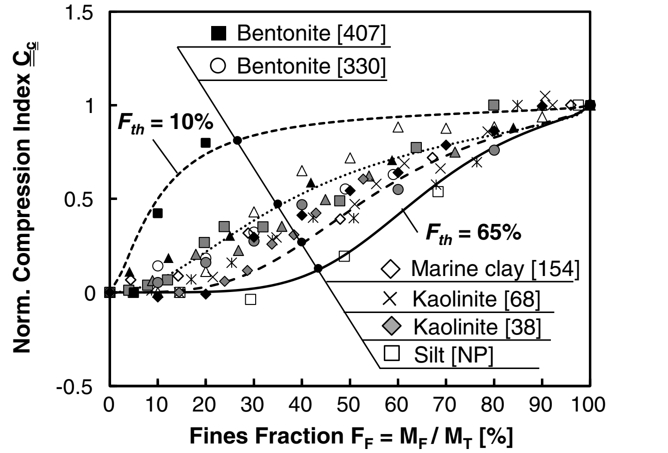

Data sources: ● Wagg and Konrad 1990; ○ Pandian et al. 1995; ■ Mollins et al. 1996; △ Kumar and Wood 1999; ◇ Monkul and Ozden 2007; □,▲,◇ Konishi et al. 2007; ✱,■,▲ Tiwari and Ajmera 2011; × Watabe et al. 2011; ◆ Simpson and Evans 2015.

Fig. 6. Normalized compression index of coarse-fine mixtures versus fines fraction by mass; the number in square brackets indicates liquid limit of fine grains; Table 1 defines the normalization and the fitting model (plotted here as lines)

This applies to the data set symbolized by the orange circle in Fig. 7(a). The normalization of $\tan\phi$ defined in Table 1 still assigns a value of 1.0 to the coarser component and 0 to the finer component.

The shear resistance of mixtures may exceed that of their components; in particular, the highest peak friction angles would be expected for highly dilative mixtures near minimum porosity [data set illustrated by the open blue square in Fig. 7(b), refer to Fig. 3].

Observations

Gravimetric-volumetric packing analyses [Fig. 2 and Eqs. (1)–(4)], the selection of low and high feasible void ratios [Eqs. (5)–(9)], and the data compilation discussed previously and detailed in Figs. 3–7 and Table 1 support the four observations that follow:

- The packing density and relative fraction of each component define the transition from coarse-controlled to fines-controlled mixtures, both for load carrying and fluid flow.
- The maximum and minimum void ratios $e^{\max}$ and $e^{\min}$ for loose and dense sands and gravels depend on the coefficient of uniformity and particle shape.
- The packing of fines depends on the liquid limit and effective stress. Three distinctive values were selected in view of near-surface engineering applications: soft at $e_F|^{10\text{ kPa}}$ and stiff at $e_F|^{1\text{ MPa}}$ for mechanical response, and viscous at $\lambda \cdot e_F|^{\text{LL}}$ for fluid flow behavior where $\lambda = [2 \cdot \log(\text{LL} - 25)]$, detailed in Eq. (9).
- Volumetric-gravimetric analyses provide the underlying conceptual framework for soil classification boundaries. However, pore filling does not necessarily occur at either $e^{\max}$ or $e^{\min}$ due to pore- and grain-scale mechanisms and processes such as the effect of boundaries that the large grains impose on the smaller grains, i.e., a function of relative size ratio (Fraser 1935). Hence, physics-inspired analytical boundaries require data-driven corrections.

These analyses and data trends reveal two critical limitations in current soil classification methods as illustrated in Fig. 1. First, the fines begin to control mechanical properties and hydraulic properties at lower fines fractions than the boundaries adopted in current soil classification systems. Second, the fixed boundaries used in existing classification methods do not account for particle shape and underestimate the impact of high-plasticity fines.

Does the gravimetric-volumetric formulation provide adequate thresholds for well-graded soils? Experimental data are scarce, and analyses provide only partial answers even for the ideal packings of spherical particles. Gravimetric-volumetric packing analyses were conducted for well-graded gravely-sandy soils, all with the same coefficient of uniformity and particle shape ($C_u = 10$ and roundness $R = 0.5$), but with different median grain size ($D_{50} =$ 3.8–204 mm). Results show a natural and gradual transition from gravel-dominant soils when the sand fraction $F_S < 10\%$, to sand-dominant behavior when the sand fraction $F_S > 48\%$. Given these results, and in the absence of negative evidence, the gravimetric-volumetric analysis proposed previously is adopted for the analysis of both gap-graded and well-graded soils (the gravimetric-volumetric analyses consider grain size of sand and gravel fractions

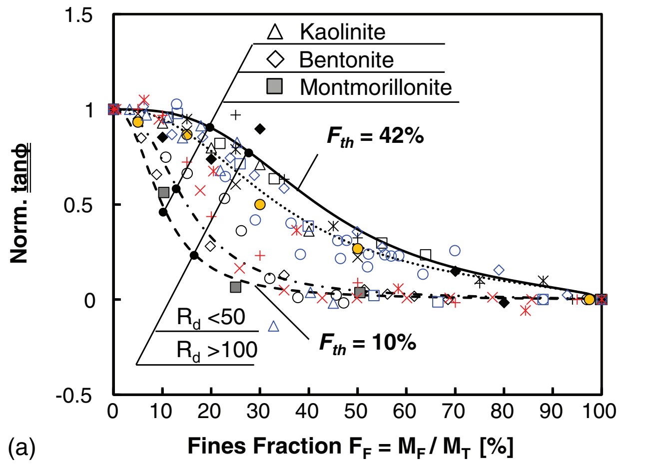

Data sources: △ Miller and Sowers 1958; ○ Kurata and Fujishita 1961; ◇ ■ Kenney 1977; □ Lupini et al. 1981; ○ Skempton 1985; □ Brown et al. 2003; + Yang 2004; × Tiwari and Marui 2005; ●: Konishi et al. 2007; ◇ Takahashi et al. 2007; △ Crawford et al. 2008; ×, ∗, + Tembe et al. 2010; ∗ Ueda et al. 2011; ◆ Simpson and Evans 2015.

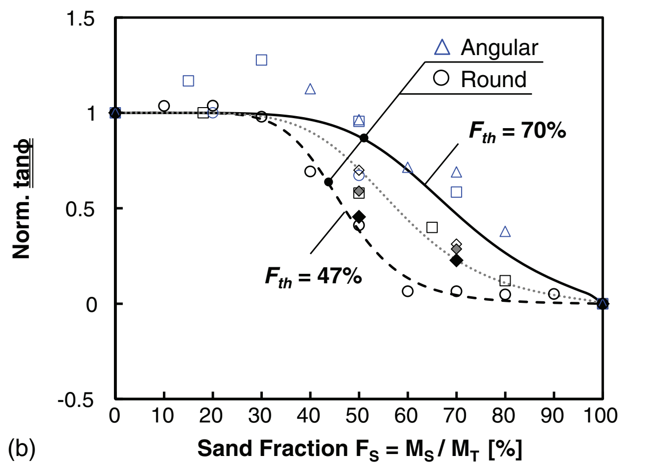

Data sources: ◇, ◇, ◆ Rathee 1981; □ Bortkevich 1982; ○ Vallejo 2001; △ Simoni and Houlsby 2006; ○ Rahardjo et al. 2008; □ Kumara et al. 2013.

Fig. 7. (Color) Normalized shear strength in terms of tan ϕ: (a) coarse-fine mixtures; (b) gravel-sand mixtures; Table 1 defines the normalization and the fitting model (plotted here as lines)

separately from each other, hence the coefficient of uniformity for the sand and gravel fractions are lower than the C_u for the whole soil mass).

Notable Mixtures and Classification Boundaries

Notable mixtures that mark the transitions between the soil components that control the mechanical response and fluid flow are now identified. These mixtures are specified in Table 2 and displayed in Fig. 8 on the textural triangle. Notable mixtures discussed subsequently assist with the definition of classification boundaries.

Mechanical Control

Densely packed soil fractions control the mechanical response of a soil. For example, the gravel carries the load in a gravel-fines mixture when the gravel packing is dense at $e_G^{\min}$ and fines are at a high void ratio $e > e_F|^{10\text{ kPa}}$; this is Mixture 1 in Table 2 and Fig. 8(a). Other notable mixtures labeled 2 and 4 follow a similar logic and procedure. Mass fractions are computed using Eqs. (1)–(9) in all cases.

Data-based thresholds F_{th} indicate that the coarse component in a mixture affects properties even when it is packed at a void ratio $e > e^{\max}$ [similar observations are in Holtz and Gibbs (1956), Vasil'eva et al. (1971), Fragaszy et al. (1992), Vallejo and Mawby (2000), Vallejo (2001), Simoni and Houlsby (2006), and Kim et al. (2007)]. Correction factors for $e^{\max}$ match the theoretically predicted threshold fractions F_F with the threshold fractions F_{th} at the arithmetic mean value observed for the various physical properties (Figs. 3–7 and Table 1). Results support the following correction factors (included in Table 2):

- Gravel-sand mixtures (Mixture 5): $\beta = 2.5$ ($e_G = \beta \cdot e_G^{\max}$; $e_S = e_S^{\min}$);
- Gravel-fines mixtures (Mixture 7): $\alpha = 1.3$ ($e_G = \alpha \cdot e_G^{\max}$; $e_F = e_F|^{1\text{ MPa}}$); and
- Sand-fines mixtures (Mixture 8): $\gamma = 1.3$ ($e_S = \gamma \cdot e_S^{\max}$; $e_F = e_F|^{1\text{ MPa}}$).

Finally, notable ternary mixtures 3, 6, and 9 are calculated as specified in Table 2. Fig. 8(a) displays all notable mixtures on the triangular chart.

These nine mixtures define boundaries for seven soil groups in terms of mechanical properties control [Fig. 8(a)]. A single component is dominant in three of the seven groups: G = gravel, S = sand, and F = fines. The four other soil groups are mixtures in transitional conditions: GS, SF, GF, and GSF. Soils that fall within the ternary transitional group GSF may exhibit distinctly different soil properties because boundaries depend on the liquid limit of fines as well as the particle shape and coefficient of uniformity of both sands and gravels.

Fluid Flow Control

Notable mixtures that define flow-control thresholds are computed using the low-viscosity criterion $e_F|^{\text{flow}} = \lambda \cdot e_F|^{\text{LL}}$ [Eq. (9)] and densely packed gravel or sand. These conditions result in Mixtures 10, 11, 12, and 13, detailed in Table 2 and plotted in Fig. 8(b).

Finally, the mixture of densely packed gravel $e_G^{\min}$ and loosely packed sand $e_S^{\max}$ are selected to define the boundary for sand-controlled hydraulic conductivity in gravel-sand mixtures [Mixture 2 in Table 2 and Fig. 8(b)].

Altogether, Mixtures 2, 10, 11, 12, and 13 delimit the three distinct zones for flow control [Fig. 8(b)]: a large region controlled by the fines (F), a smaller region controlled by the sand (S), and the corner reserved for clean gravels (G).

Classification: Charts

Classification Groups and Nomenclature

Distinct differences between the textural charts for mechanical behavior control [Fig. 8(a)] and for flow control [Fig. 8(b)] suggest the need for a two-name nomenclature whereby the first letters identify the component that controls mechanical properties, followed by a letter that identifies the component that controls flow (shown in parenthesis). For example, consider a S(F) soil: sand controls the mechanical properties but fines control its hydraulic conductivity.

The resulting 10 soil groups are summarized in Fig. 9. The fines fraction in F, GF, SF, and GSF soils controls the hydraulic conductivity in these groups. While the two-name nomenclature F(F), GF (F), SF(F), and GSF(F) is redundant in these cases, it clearly states the distinct role of fines on both mechanical and flow properties. Clean gravel G(G) and clean sand S(S) classifications can be

Table 2. Notable Mixtures Used to Define Soil Classification Boundaries

Process	Controlling fraction	Mixture number	Packing condition: Gravel	Sand	Fines	Physical background: interpretation
Load carrying	Gravel	1	$e_G^{\min}$	—	$e_F\|^{10\ \mathrm{kPa}}$	Gravels carry the load if gravels are densely packed and fines experience $\sigma' < 10$ kPa
		2	$e_G^{\min}$	$e_S^{\max}$	—	Gravels carry the load if gravels are densely packed and sands are loosely packed
		3	$e_G^{\min}$	$e_S^{\max}$	$e_F\|^{10\ \mathrm{kPa}}$	Gravels carry the load if gravels are densely packed, sands are loose, and fines experience $\sigma' < 10$ kPa
	Sand	4	—	$e_S^{\min}$	$e_F\|^{10\ \mathrm{kPa}}$	Sands carry the load if sands are densely packed and fines experience $\sigma' < 10$ kPa
		5	$2.5e_G^{\max}$	$e_S^{\min}$	—	Sands carry the load if sands are densely packed and contain very loose gravel at $2.5e_G^{\max}$
		6	$2.5e_G^{\max}$	$e_S^{\min}$	$e_F\|^{10\ \mathrm{kPa}}$	Sands carry the load if sands are densely packed and contain very loose gravel at $2.5e_G^{\max}$ and soft fines
	Fines	7	$1.3e_G^{\max}$	—	$e_F\|^{1\ \mathrm{MPa}}$	Fines carry the load when they are compact and contain loose gravel at $1.3e_G^{\max}$
		8	—	$1.3e_S^{\max}$	$e_F\|^{1\ \mathrm{MPa}}$	Fines carry the load when they are compact and contain loosely packed sand at $1.3e_S^{\max}$
		9	$2.5e_G^{\max}$	$1.3e_S^{\max}$	$e_F\|^{1\ \mathrm{MPa}}$	Fines carry the load when they are compact and contain very loose gravels and sands
Fluid flow	Fines	10	$e_G^{\min}$	—	$\lambda e_F\|^{\mathrm{LL}}$	The fraction for clean gravels and sands is computed by assuming that the coarse fraction is at $e^{\min}$ and that fines form a high-viscosity fluid at a water content equal to λLL, i.e., the void ratio of fines is $e_F\|^{\mathrm{flow}} = \lambda e_F\|^{\mathrm{LL}}$ where $\lambda = [2\log(\mathrm{LL}-25)]$
		11	$e_G^{\min}$	$e_S^{\max}$	$\lambda e_F\|^{\mathrm{LL}}$	
		12	$2.5e_G^{\max}$	$e_S^{\min}$	$\lambda e_F\|^{\mathrm{LL}}$	
		13	—	$e_S^{\min}$	$\lambda e_F\|^{\mathrm{LL}}$	

Note: F = fines; G = gravel; S = sand; estimates: values of $e^{\max}$, $e^{\min}$, $e_F|^{10\ \mathrm{kPa}}$, $e_F|^{1\ \mathrm{MPa}}$, and $e_F|^{\mathrm{LL}}$ can be estimated from index properties [Eqs. (5)–(9)].

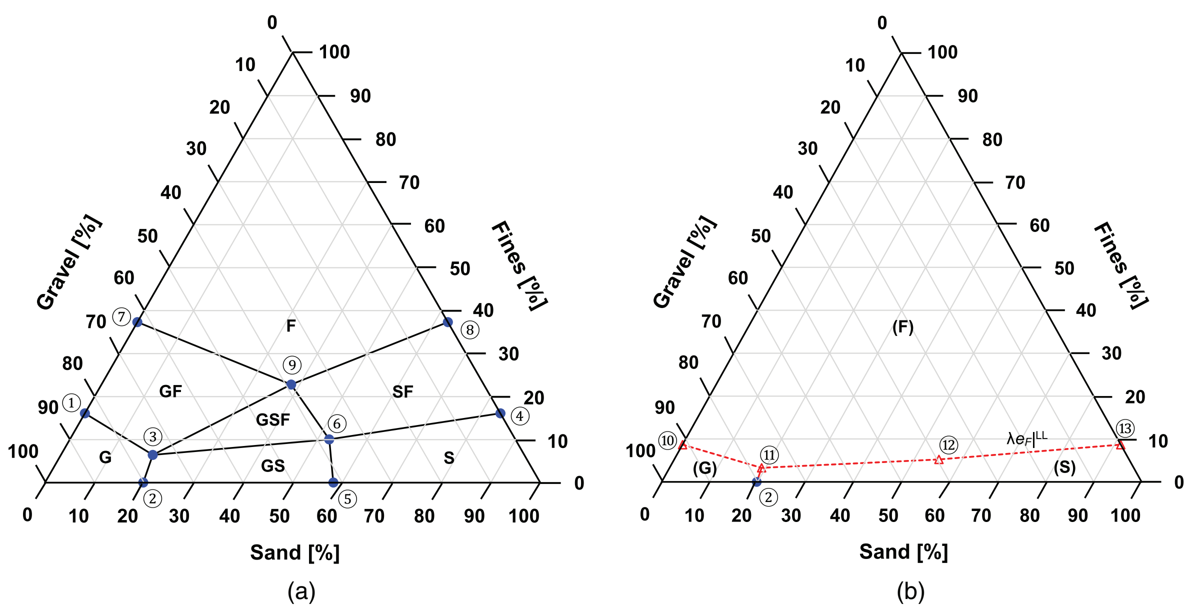

Fig. 8. (Color) Notable mixtures and soil classification boundaries; G = gravel, S = sand, and F = fines: (a) mechanical control: G, S, and F indicate that a single fraction controls the mechanical response zone, GF, SF, GS, and GSF designate transition zones; (b) flow control: fluid flow controlling fraction denoted as a single letter between parentheses; soil properties used for this chart: angular and uniform gravel $e_G^{\max} = 0.81$ and $e_G^{\min} = 0.45$; angular and uniform sand $e_S^{\max} = 0.81$ and $e_S^{\min} = 0.45$; fines resemble kaolinite with liquid limit LL = 50, $e_F|^{10\ \mathrm{kPa}} = 1.33$, $e_F|^{1\ \mathrm{MPa}} = 0.76$, $e_F|^{\mathrm{LL}} = 1.32$, and $\lambda = 2.8$; flow-controlling fine fractions are $F_F = 3.3\%$ at Mixture 11 and $F_F = 5.2\%$ at Mixture 12

augmented with the well-graded or poorly graded qualifiers used in the USCS.

Sample Charts

Charts in Fig. 10 capture mechanical-control and flow-control boundaries superimposed onto a single chart for each case. These charts reflect a wide range of soil conditions and include both angular-uniform and rounded-well-graded sands and gravels, in addition to fines of varying plasticity.

Threshold fractions are markedly different from those used in the USCS. For various combinations of roundness, coefficients of uniformity, and fines plasticity, results indicate

Needed Input			
Gravel G	Fraction F_G	e_G^{max} and e_G^{min}	or roundness R and uniformity C_u
Sand S	Fraction F_S	e_S^{max} and e_S^{min}	or roundness R and uniformity C_u
Fines F	Fraction F_F	$e_F\|^{10kPa}$, $e_F\|^{1MPa}$, and $e_F\|^{LL}$	or liquid limit LL

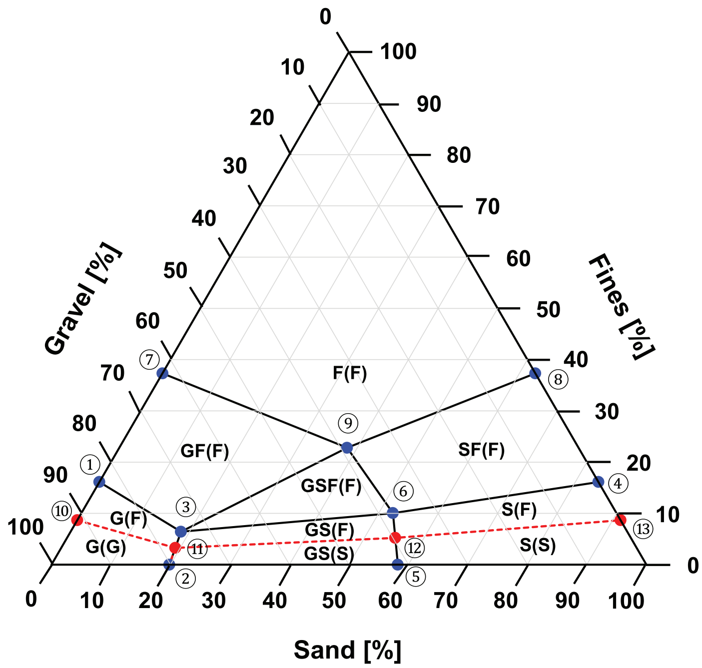

Group	Controlling Fraction		Description
	Mechanical Response	Fluid Flow	
F(F)	Fines	Fines	Fine-grained soil
GF(F)	Gravel & Fines	Fines	Transitional Mixture
SF(F)	Sand & Fines	Fines	Transitional Mixture
GS(F)	Gravel & Sand	Fines	Transitional Mixture
GSF(F)	Gravel-Sand-Fines	Fines	Transitional Mixture
G(F)	Gravel	Fines	Gravel with Fines
S(F)	Sand	Fines	Sand with Fines
G(G)*	Gravel	Gravel	Clean Gravel
S(S)*	Sand	Sand	Clean Sand
GS(S)	Gravel & Sand	Sand	Clean Gravel-Sand Mixture

Notes:

- (*) Specify well-graded or poorly-graded (Refer USCS). Well-graded G(G): $C_u \geq 4$ and $1 \leq C_c \leq 3$. Well-graded S(S): $C_u \geq 6$ and $1 \leq C_c \leq 3$.
- A soil group F or (F): Classify fines according to plasticity and sensitivity to pore-fluid chemistry.
- Recommendation: including triangular textural charts as part of standard reporting practice.

Fig. 9. (Color) Soil classification boundaries: mechanical control (blue points) and fluid flow control (red points); soil properties used for this chart: angular and uniform gravel $e_G^{\max} = 0.81$ and $e_G^{\min} = 0.45$; angular and uniform sand $e_S^{\max} = 0.81$ and $e_S^{\min} = 0.45$; fines resemble kaolinite with liquid limit LL $= 50$, $e_F|^{10\text{ kPa}} = 1.33$, $e_F|^{1\text{ MPa}} = 0.76$, $e_F|^{\text{LL}} = 1.32$, and $\lambda = 2.8$; flow-controlling fine fractions are $F_F = 3.3\%$ at Mixture 11 and $F_F = 5.2\%$ at Mixture 12

- Gravel-sand mixtures: threshold sand fractions range between $F_S|^L = 12$–24% and $F_S|^H = 45$–65%;
- Coarse-fine mixtures, mechanical control: the fines threshold varies between $F_F|^L = 3$–27% and $F_F|^H = 12$–50%; and
- Coarse-fine mixtures, flow control: the fines threshold varies from $F_F|^{\text{flow}} = 1$–23%.

The predominant role of fines extends much further into the lower fines content than anticipated by the USCS [compare the RSCS charts in Fig. 10 with the USCS chart in Fig. 1(b)]. In fact, the USCS has the closest resemblance to the triangular textural chart computed for low-plasticity fines (such as kaolinite), and angular sands and gravels. Fines plasticity plays a critical role in the position of boundaries for both mechanical and hydraulic controls. In particular, well-graded rounded sands and gravels can form denser packings than uniform angular coarse grains, therefore a small mass fraction of fines is needed to alter soil behavior in this case [e.g., compare classification charts in Figs. 10(a–d) against Figs. 10(e–h)].

These new classification charts incorporate the main parameters used by the USCS, that is, Sieves No. 200 and No. 4, coefficient of uniformity C_u, and liquid limit LL of fines (the values of $e^{\max}$ and $e^{\min}$ implicitly consider the coefficient of curvature). Furthermore,

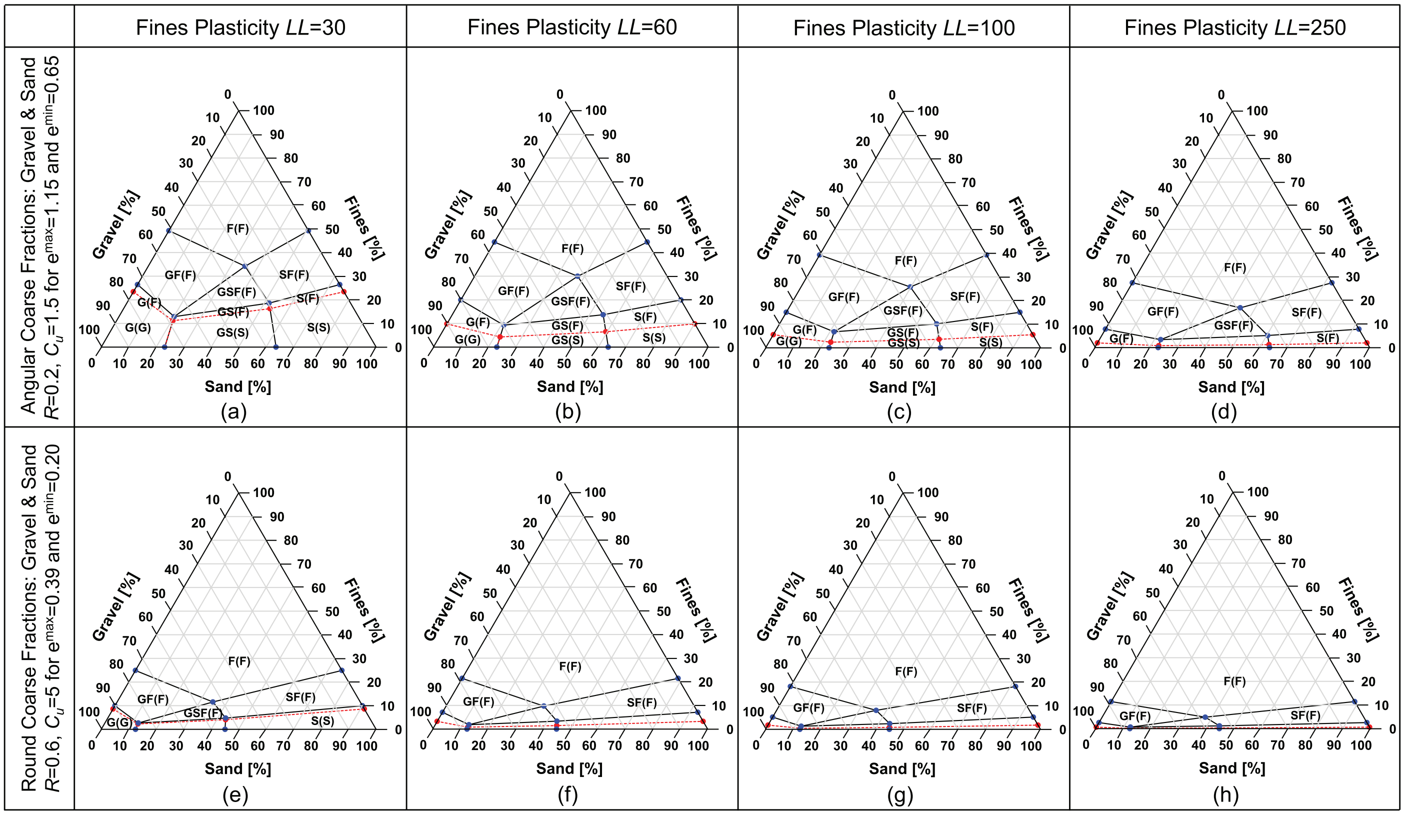

Fig. 10. (Color) Revised soil classification system sample charts: angular gravel and sand with (a) fines LL = 30, (b) fines LL = 60, (c) fines LL = 100, and (d) fines LL = 250; round gravel and sand with (e) fines LL = 30, (f) fines LL = 60, (g) fines LL = 100, and (h) fines LL = 250; refer to Fig. 9 for missing nomenclature in small zones

the development of these charts recognizes the role of particle shape on the behavior of sands and gravels. It also considers the stress regime to which the soil will be subjected in near-surface geotechnical engineering projects.

Fines Classification

The classification of fines could be completed using the standard Casagrande chart in the USCS. However, the revised classification RSCS adopts the new fines classification method proposed by Jang and Santamarina (2016) because it takes into consideration both the soil plasticity and its sensitivity to pore fluid chemistry. This classification is based on liquid limits obtained with deionized water, brine (high electrical conductivity), and kerosene (low dielectric constant). Fines fall into 1 of 12 groups: NL, NI, NH, LL, LI, LH, IL, II, IH, HL, HI, and HH, where the first letter indicates the soil plasticity (no, low, intermediate, high) and the second letter indicates the sensitivity of the soil response to changes in pore fluid chemistry (low, intermediate, high).

Revised Soil Classification System

The recommended procedure for soil classification follows:

1. Input parameters:
   a. Obtain the gravel fraction F_G (where $G >$ Sieve No. 4), sand fraction F_S (Sieve No.200 < S < Sieve No. 4) and fines fraction F_S (passing Sieve No. 200) by mass;
   b. For gravel and for sand: Determine e^{max} and e^{min} for each fraction. For estimates of e^{max} and e^{min}, use the coefficient of uniformity C_u and roundness R gathered for each fraction [Eqs. (5) and (6)]; and
   c. For fines: Determine $e_F|^{10\ \mathrm{kPa}}$, $e_F|^{1\ \mathrm{MPa}}$, and $e_F|^{\mathrm{LL}}$ or estimate these values from the liquid limit measured on the passing Sieve No. 200 using the pore fluid that the soil is subjected to in the field [Eqs. (7)–(9)].
2. Classification chart: Compute a case specific chart using the notable Mixtures 1–13 specified in Table 2. Computations and graphing schemes are built into Figs. S1 and S2:
   a. Determine the boundaries for the load-carrying component (Mixtures 1–9, Table 2); and
   b. Determine the boundaries for the flow-controlling component (Mixtures 10–13, Table 2).
3. Soil Classification: Alternatively, select the textural triangular chart in Fig. 10 that most closely resembles the soil under consideration. Plot the point that corresponds to the soil under consideration and determine its classification using the two-name nomenclature suggested previously: the first letter(s) indicates the load-carrying component, followed by a letter in parenthesis that denotes the component that controls flow. When appropriate, include the RSCS triangular chart as part of the report.
4. Fines classification: Follow the classification procedure described in Jang and Santamarina (2016) to consider the fines plasticity and sensitivity to changes in pore fluid chemistry. This method requires additional liquid limit determinations for soil pastes mixed with brine and kerosene.

Conclusions

Soil classification is intended to help geotechnical engineers anticipate the properties and behavior of soils by grouping them into similar response categories based on index properties. Soil classification systems worldwide capture great physical insight. Yet, analyses and data trends reveal critical limitations in the boundaries for various soil groups adopted in classical soil classification systems. In particular, fines begin to play a significant role at threshold fractions that are smaller than boundaries adopted by the existing classification systems.

Classification boundaries can be defined by the void ratio that each fraction may attain. The revised classification adopts $e^{\max}$ and $e^{\min}$ for gravels and sands, and three distinctive values for fines: soft $e_F|^{10\text{ kPa}}$ and stiff $e_F|^{1\text{ MPa}}$ for the mechanical response, and viscous $\lambda e_F|^{\text{LL}}$ for the fluid flow behavior where $\lambda = [2 \cdot \log(\text{LL} - 25)]$. There are robust correlations between these void ratios and index properties such as particle shape, coefficient of uniformity, and liquid limit.

Analytically computed and data-adjusted threshold fractions point to very different values to those used as boundaries in the Unified Soil Classification System, both for mechanical control and for flow control. The boundaries in the USCS have some—albeit limited—resemblance to the RSCS boundaries computed for low-plasticity clays (such as kaolinite) and angular sands and gravels.

Threshold fractions for mechanical control and for flow control are quite distinct. The RSCS uses a two-name nomenclature whereby the first letters identify the component that controls mechanical properties, followed by a letter shown in parenthesis that identifies the component that controls flow.

Finally, the detailed classification of fines uses the new fines classification method proposed by Jang and Santamarina (2016) that takes into consideration the plasticity of fines and their sensitivity to pore fluid chemistry.

Appendix. Volumetric-Gravimetric Relations

Binary Mixtures: Fines Fraction

Consider a binary mixture made of coarse and fine fractions. The coarse grains are packed at a void ratio e_C. The volume of voids between coarse grains V_{vC} is related to the volume of solids V_{sC} through the void ratio e_C

$$V_{vC} = e_C V_{sC} \tag{11}$$

Fine grains packed at void ratio e_F fill the volume of voids between coarse grains V_{vC}. Then, the volume of solids in the fine grains V_{sF} is

$$V_{sF} = \frac{V_{vC}}{1 + e_F} = \frac{e_C}{1 + e_F} V_{sC} \tag{12}$$

Define the mass fraction of fines as the mass of fines M_F divided by the total mass of fines and coarse fractions $M_F + M_C$; then

$$F_F = \frac{M_F}{M_F + M_C} = \frac{1}{1 + \frac{M_C}{M_F}} = \frac{1}{1 + \frac{G_{sC}}{G_{sF}} \frac{V_{sC}}{V_{sF}}} \tag{13}$$

where G_{sC} and G_{sF} are the specific gravities of coarse and fine fractions. Replacing Eq. (12) in Eq. (13) gives

$$F_F = \frac{1}{1 + \frac{G_{s,C}}{G_{s,F}} \frac{1+e_F}{e_C}} \approx \frac{e_C}{1 + e_C + e_F} \tag{14}$$

(the approximation applies to $G_{sC} \approx G_{sF}$)

The same equation can be used for gravel-sand, gravel-fines, and sand-fines mixtures.

Ternary Mixture: Gravel, Sand, and Fines Fractions

Extend the analysis to ternary gravel-sand-fines mixtures, where the gravel is packed at void ratio e_G. The sand packed at void ratio e_S fills the voids in the gravel V_{vG}. The remaining volume of voids is filled by the fines packed at void ratio e_F. From Eqs. (12) and (13)

$$M_F = \frac{e_S}{1 + e_F} M_S \left(\frac{G_{sF}}{G_{sS}}\right) \tag{15}$$

$$M_S = \frac{e_G}{1 + e_S} M_G \left(\frac{G_{sS}}{G_{sG}}\right) \tag{16}$$

Finally, the mass fraction of gravel F_G, sand F_S, and fines F_F relative to the total mass $M_G + M_S + M_F$ is obtained by successively invoking the previous two equations, Eqs. (15) and (16). For clarity, consider $G_{sG} \approx G_{sS} \approx G_{sF}$

$$F_G = \frac{M_G}{M_G + M_S + M_F} = \frac{1}{\left(1 + \frac{e_G}{1+e_S} + \frac{e_S}{1+e_F}\frac{e_G}{1+e_S}\right)} \tag{17}$$

$$F_S = \frac{M_S}{M_G + M_S + M_F} = \frac{1}{\left(\frac{1+e_S}{e_G} + 1 + \frac{e_S}{1+e_F}\right)} \tag{18}$$

$$F_F = \frac{M_f}{M_G + M_S + M_F} = \frac{1}{\left(\frac{1+e_S}{e_G}\frac{1+e_F}{e_S} + \frac{1+e_F}{e_S} + 1\right)} \tag{19}$$

Note that $F_G + F_S + F_F = 1.0$.

Acknowledgments

Support for this research was provided by the KAUST Endowment at King Abdullah University of Science and Technology. G. Abelskamp edited the manuscript. We are grateful to the anonymous reviewers for their detailed comments and valuable insights.

Supplemental Data

Figs. S1 and S2 are available online in the ASCE Library (www.ascelibrary.org).

References

Association Suisse de Normalization (Swiss Association for Normalization). (1959). "Soil classification." *SNV 70 055*, Zurich, Switzerland.

ASTM. (2009). "Standard practice for classification of soils and soil-aggregate mixtures for highway construction purposes." *ASTM D3282*, West Conshohocken, PA.

ASTM. (2011). "Standard practice for classification of soils for engineering purposes (unified soil classification system)." *ASTM D2487*, West Conshohocken, PA.

Bandini, P., and Sathiskumar, S. (2009). "Effects of silt content and void ratio on the saturated hydraulic conductivity and compressibility of sand-silt mixtures." *J. Geotech. Geoenviron. Eng.*, 10.1061/(ASCE)GT.1943-5606.0000177, 1976–1980.

Bareither, C. A., Edil, T. B., Benson, C. H., and Mickelson, D. M. (2008). "Geological and physical factors affecting the friction angle of compacted sands." *J. Geotech. Geoenviron. Eng.*, 10.1061/(ASCE)1090-0241(2008)134:10(1476), 1476–1489.

Belkhatir, M., Schanz, T., and Arab, A. (2013). "Effect of fines content and void ratio on the saturated hydraulic conductivity and undrained shear strength of sand-silt mixtures." *Environ. Earth. Sci.*, 70(6), 2469–2479.

Bortkevich, S. V. (1982). "Density of placing sand-gravel and pebble soils in dams." *Power Technol. Eng.*, 16(6), 324–328.

Brown, K. M., Kopf, A., Underwood, M. B., and Weinberger, J. L. (2003). "Compositional and fluid pressure controls on the state of stress on the Nankai subduction thrust: A weak plate boundary." *Earth. Planet. Sci. Lett.*, 214(3), 589–603.

BSI (British Standards Institution). (1999). "Code of practice for site investigations." *BS 5930*, London.

Burland, J. B. (1990). "On the compressibility and shear strength of natural clays." *Géotechnique*, 40(3), 329–378.

Casagrande, A. (1948). "Classification and identification of soils." *Trans. ASCE*, 113(1), 901–930.

Chinese Standard. (2007). "Standard for engineering classification of soil." *GBT 50145*, China Planning Press, Beijing.

Cho, G. C., Dodds, J., and Santamarina, J. C. (2006). "Particle shape effects on packing density, stiffness, and strength: Natural and crushed sands." *J. Geotech. Geoenviron. Eng.*, 10.1061/(ASCE)1090-0241(2006)132:5(591), 591–602.

Chong, S. H., and Santamarina, J. C. (2016). "Soil compressibility models for a wide stress range." *J. Geotech. Geoenviron. Eng.*, 10.1061/(ASCE)GT.1943-5606.0001482, 06016003.

Choo, H. (2013). "Engineering behavior and characterization of physical-chemical particulate mixture using geophysical measurement techniques." Ph.D. thesis, Georgia Institute of Technology, Atlanta.

Crawford, B. R., Faulkner, D. R., and Rutter, E. H. (2008). "Strength, porosity, and permeability development during hydrostatic and shear loading of synthetic quartz-clay fault gouge." *J. Geophys. Res - Solid Earth*, 113(B3), B03207.

Das, M. D. (2009). *Principles of geotechnical engineering*, Cengage Learning, Stamford, CT.

Deutche Norm. (2011). "Erd-und grundbau—bodenklassifikationfür-bautechnischezwecke." *DIN 18196*, BeuthVerlag GmbH, Berlin.

Donohue, T. (2008). "Permeability and the structure of porosity in particulate materials." Ph.D. thesis, Univ. of Newcastle, Callaghan, Australia.

Dundulis, K., Gadeikis, S., Gadeikytė, S., Urbaitis, D., and Prunskienė, L. (2010). "Problems of usage of soil classification systems for sand soils of Lithuania." *10th Int. Conf*, Vilnius Gediminas Technical Univ., Vilnius, Lithuania.

Evans, T. M., and Valdes, J. R. (2011). "The microstructure of particulate mixtures in one-dimensional compression: Numerical studies." *Granular Matter*, 13(5), 657–669.

Fourie, A. B., and Papageorgiou, G. (2001). "Defining an appropriate steady state line for Merriespruit gold tailings." *Can. Geotech. J.*, 38(4), 695–706.

Fragaszy, R. J., Su, J., Siddiqi, F. H., and Ho, C. L. (1992). "Modeling strength of sandy gravel." *J. Geotech. Eng.*, 10.1061/(ASCE)0733-9410(1992)118:6(920), 920–935.

Fraser, H. J. (1935). "Experimental study of the porosity and permeability of clastic sediments." *J. Geol.*, 43(8), 910–1010.

Guyon, E., Oger, L., and Plona, T. J. (1987). "Transport properties in sintered porous media composed of two particle sizes." *J. Phys. D-Appl Phys.*, 20(12), 1637–1644.

Han, D. H., Nur, A., and Morgan, D. (1986). "Effects of porosity and clay content on wave velocities in sandstones." *Geophysics*, 51(11), 2093–2107.

Holtz, W. G., and Gibbs, H. J. (1956). "Triaxial shear tests on pervious gravelly soils." *J. Soil Mech. Found. Div.*, 82(1), 1–22.

Howard, A. K. (1984). "The revised ASTM standard on the unified classification system." *Geotech. Test. J.*, 7(4), 216–222.

Indrawan, I. G. B., Rahardjo, H., and Leong, E. C. (2006). "Effects of coarse-grained materials on properties of residual soil." *Eng. Geol.*, 82(3), 154–164.

Istomina, V. S. (1957). "*Seepage stability of the soil*." Gosstroiizdat, Moscow.

Jang, J., and Santamarina, J. C. (2016). "Fines classification based on sensitivity to pore-fluid chemistry." *J. Geotech. Geoenviron. Eng.*, 10.1061/(ASCE)GT.1943-5606.0001420, 06015018.

Japanese Geotechnical Society. (2009). "Method of classification of geomaterials for engineering purposes." *JGS0051*, Tokyo.

Kamann, P. J., Ritzi, R. W., Dominic, D. F., and Conrad, C. M. (2007). "Porosity and permeability in sediment mixtures." *Groundwater*, 45(4), 429–438.

Kang, M., and Lee, J. S. (2015). "Evaluation of the freezing-thawing effect in sand-silt mixtures using elastic waves and electrical resistivity." *Cold Reg. Sci. Technol.*, 113, 1–11.

Kenney, T. C. (1967). "The influence of mineral composition on the residual strength of natural soils." *Proc., Geotech. Conf.*, Vol. 1, Norwegian Geotechnical Institute, Oslo, Norway, 123–129.

Kenney, T. C. (1977). "Residual strengths of mineral mixtures." Dept. of Civil Engineering, Univ. of Toronto, Toronto.

Kenney, T. C., and Lau, D. (1985). "Internal stability of granular filters." *Can. Geotech. J.*, 22(2), 215–225.

Kim, H. K., Cortes, D. D., and Santamarina, J. C. (2007). "Flow test: Particle-level and macroscale analyses." *ACI Mater. J.*, 104(3), 323–327.

Knoll, M. D., and Knight, R. (1994). "Relationships between dielectric and hydrogeologic properties of sand–clay mixtures." *Proc., 5th Int. Conf. Ground Penetrating Radar*, Kitchener, ON, Canada, 45–61.

Koltermann, C. E., and Gorelick, S. M. (1995). "Fractional packing model for hydraulic conductivity derived from sediment mixtures." *Water Resour. Res.*, 31(12), 3283–3297.

Konishi, Y., Hyodo, M., and Ito, S. (2007). "Compression and undrained shear characteristics of sand-fines mixtures with various plasticity." *J. Geotech. Geoenviron. Eng.*, 63(4), 1142–1152 (in Japanese).

Kovačević, M. S., and Jurić-Kaćunić, D. (2014). "European soil classification system for engineering purposes." *Građevinar*, 66(9), 801–810.

Krumbein, W. C., and Sloss, L. L. (1963). *Stratigraphy and sedimentation*, 2nd Ed., Freeman and Company, San Francisco.

Kumar, G. V., and Wood, D. M. (1999). "Fall cone and compression tests on clay-gravel mixtures." *Geotechnique*, 49(6), 727–739.

Kumara, J., Hayano, K., Shigekuni, Y., and Sasaki, K. (2013). "Physical and mechanical properties of sand-gravel mixtures evaluated from DEM simulation and laboratory triaxial test." *Int. J. GEOMATE.*, 4(2), 546–551.

Kurata, S., and Fujishita, T. (1961). "Research on the engineering properties of sand-clay mixtures." *Rep. Port Harbour Res. Inst.*, 11(9), 389–424.

Lade, P. V., and Yamamuro, J. A. (1997). "Effects of nonplastic fines on static liquefaction of sands." *Can. Geotech. J.*, 34(6), 918–928.

Lee, H., and Koo, S. (2014). "Liquid permeability of packed bed with binary mixture of particles." *J. Ind. Eng. Chem.*, 20(4), 1397–1401.

Lee, J. S., Dodds, J., and Santamarina, J. C. (2007a). "Behavior of rigid-soft particle mixtures." *J. Mater. Civ. Eng.*, 10.1061/(ASCE)0899-1561(2007)19:2(179), 179–184.

Lee, J. S., Guimaraes, M., and Santamarina, J. C. (2007b). "Micaceous sands: Microscale mechanisms and macroscale response." *J. Geotech. Geoenviron. Eng.*, 10.1061/(ASCE)1090-0241(2007)133:9(1136), 1136–1143.

Li, Y. (2009). "Experimental study of shear behavior of soils with abundant coarse particles associated with slip zones of large landslides in the three gorges reservoir." Ph.D. thesis, Univ. of Hong Kong, Hong Kong.

Locat, J., and Demers, D. (1988). "Viscosity, yield stress, remolded strength, and liquidity index relationships for sensitive clays." *Can. Geotech. J.*, 25(4), 799–806.

Lupini, J. F., Skinner, A. E., and Vaughan, P. R. (1981). "The drained residual strength of cohesive soils." *Geotechnique*, 31(2), 181–213.

Maio, C. D., and Fenellif, G. B. (1994). "Residual strength of kaolin and bentonite: The influence of their constituent pore fluid." *Geotechnique*, 44(2), 217–226.

Marion, D., Nur, A., Yin, H., and Han, D. H. (1992). "Compressional velocity and porosity in sand-clay mixtures." *Geophysics*, 57(4), 554–563.

Marion, D. P. (1990). "Acoustical, mechanical, and transport properties of sediments and granular materials." Ph.D. thesis, Stanford Univ., Palo Alto, CA.

Mason, T. (1997). "Hydrodynamics and sediment transport on a macro-tidal, mixed (sand and shingle) beach." Ph.D. thesis, Univ. of Southampton, Southampton, U.K.

McGeary, R. K. (1961). "Mechanical packing of spherical particles." *J. Am. Ceram. Soc.*, 44(10), 513–522.

Miller, E. A., and Sowers, G. F. (1958). "The strength characteristics of soil-aggregate mixtures and discussion." *Highway Res. Board Bull.*, 16–32.

Mitchell, J. K., and Soga, K. (2005). *Fundamentals of soil behavior*, Wiley, Hoboken, NJ.

Mollins, L. H., Stewart, D. I., and Cousens, T. W. (1996). "Predicting the properties of bentonite-sand mixtures." *Clay Miner.*, 31(2), 243–252.

Monkul, M. M., and Ozden, G. (2007). "Compressional behavior of clayey sand and transition fines content." *Eng. Geol.*, 89(3), 195–205.

Palomino, A. M., and Santamarina, J. C. (2005). "Fabric map for kaolinite: Effects of pH and ionic concentration on behavior." *Clays Clay Miner.*, 53(3), 211–223.

Pandian, N. S., Nagaraj, T. S., and Raju, P. N. (1995). "Permeability and compressibility behavior of bentonite-sand/soil mixes." *ASTM Geotech. Test. J.*, 18(1), 86–93.

Pennekamp, J. G. S., Talmon, A. M., and van Kesteren, W. G. M. (2010). "Determination of non-segregating tailings conditions." *Proc., Wodcon XIX*, World Organisation of Dredging Associations, Spotsylvania, VA, 848–858.

Radjai, F., Wolf, D. E., Jean, M., and Moreau, J. J. (1998). "Bimodal character of stress transmission in granular packing." *Phys. Rev. Lett.*, 80(1), 61–64.

Rahardjo, H., Indrawan, I. G. B., Leong, E. C., and Yong, W. K. (2008). "Effects of coarse-grained material on hydraulic properties and shear strength of top soil." *Eng. Geol.*, 101(3), 165–173.

Rathee, R. K. (1981). "Shear strength of granular soils and its prediction by modeling techniques." *J. Inst. Eng.*, 62, 64–70.

Salgado, R., Bandini, P., and Karim, A. (2000). "Shear strength and stiffness of silty sand." *J. Geotech. Geoenviron. Eng.*, 10.1061/(ASCE)1090-0241(2000)126:5(451), 451–462.

Santamarina, J. C., and Cho, G. C. (2004). "Soil behaviour: The role of particle shape." *Advances in Geotechnical Engineering: The Skempton Conf.*, R. J. Jardine, D. M. Potts, and K. G. Higgins, eds., Vol. 1, Thomas Telford, London, 604–617.

Santamarina, J. C., Klein, K. A., and Fam, M. A. (2001). *Soils and waves: Particulate materials behavior, characterization and process monitoring*, Wiley, Chichester, U.K.

Santamarina, J. C., and Shin, H. (2009). "Friction in granular media." *Meso-scale shear physics in earthquake and landslide mechanics*, CRC Press, London, 157–188.

Schofield, A. N. (1980). "Cambridge geotechnical centrifuge operations." *Geotechnique*, 30(3), 227–268.

SETRA and LCPC (SETRA-Road and highway technical studies office and LCPC-Central Laboratory for Roads and Bridges, a French public research institution). (2000). "GTR (Guide Technique Réalisation des remblais et couches de forme)." fascicule I., SETRA-LCPC (Service d'Etudes Techniques des Routes et Autoroutes-Laboratoire Central des Ponts et Chaussées), France.

Shafiee, A. (2008). "Permeability of compacted granule-clay mixtures." *Eng. Geol.*, 97(3), 199–208.

Shelley, T. L., and Daniel, D. E. (1993). "Effect of gravel on hydraulic conductivity of compacted soil liners." *J. Geotech. Eng.*, 10.1061/(ASCE)0733-9410(1993)119:1(54), 54–68.

Shire, T., O'Sullivan, C., Hanley, K. J., and Fannin, R. J. (2014). "Fabric and effective stress distribution in internally unstable soils." *J. Geotech. Geoenviron. Eng.*, 10.1061/(ASCE)GT.1943-5606.0001184, 04014072.

Simoni, A., and Houlsby, G. T. (2006). "The direct shear strength and dilatancy of sand-gravel mixtures." *Geotech. Geol. Eng.*, 24(3), 523–549.

Simpson, D. C., and Evans, T. M. (2015). "Behavioral thresholds in mixtures of sand and kaolinite clay." *J. Geotech. Geoenviron. Eng.*, 10.1061/(ASCE)GT.1943-5606.0001391, 04015073.

Sivapullaiah, P. V., Sridharan, A., and Stalin, V. K. (2000). "Hydraulic conductivity of bentonite-sand mixtures." *Can. Geotech. J.*, 37(2), 406–413.

Skempton, A. W. (1985). "Residual strength of clays in landslides, folded strata and the laboratory." *Geotechnique*, 35(1), 3–18.

Skempton, A. W., and Brogan, J. M. (1994). "Experiments on piping in sandy gravels." *Geotechnique*, 44(3), 449–460.

Skempton, A. W., and Jones, O. T. (1944). "Notes on the compressibility of clays." *Q. J. Geol. Soc.*, 100(1–4), 119–135.

Sridharan, A., and Nagaraj, H. B. (2000). "Compressibility behaviour of remoulded, fine-grained soils and correlation with index properties". *Can. Geotech. J.*, 37(3), 712–722.

Steiakakis, E., Gamvroudis, C., Komodromos, A., and Repouskou, E. (2012). "Hydraulic conductivity of compacted kaolin–sand specimens under high hydraulic gradients." *Electronic J. Geotech. Eng.*, 17, 783–799.

Takahashi, M., Mizoguchi, K., Kitamura, K., and Masuda, K. (2007). "Effects of clay content on the frictional strength and fluid transport property of faults." *J. Geophys. Res. Solid Earth*, 112(B8), B08206.

Tanaka, T., and Toida, M. (2008). "Characteristics and method of estimating permeability of bentonite-sand-gravel mixture." *Doboku Gakkai Ronbunshuu C (Online)*, 64(1), 101–110.

Tembe, S., Lockner, D. A., and Wong, T. F. (2010). "Effect of clay content and mineralogy on frictional sliding behavior of simulated gouges: Binary and ternary mixtures of quartz, illite, and montmorillonite." *J. Geophys. Res: Solid Earth*, 115(B3), B03416.

Thevanayagam, S. (2007). "Intergrain contact density indices for granular mixes—I: Framework." *J. Earthquake Eng. Eng. Vibr.*, 6(2), 123–134.

Thevanayagam, S., Shenthan, T., Mohan, S., and Liang, J. (2002). "Undrained fragility of clean sands, silty sands, and sandy silts." *J. Geotech. Geoenviron. Eng.*, 10.1061/(ASCE)1090-0241(2002)128:10(849), 849–859.

Tiwari, B., and Ajmera, B. (2011). "Consolidation and swelling behavior of major clay minerals and their mixtures." *Appl. Clay Sci.*, 54(3), 264–273.

Tiwari, B., and Marui, H. (2005). "A new method for the correlation of residual shear strength of the soil with mineralogical composition." *J. Geotech. Geoenviron. Eng.*, 10.1061/(ASCE)1090-0241(2005)131:9(1139), 1139–1150.

Ueda, T., Matsushima, T., and Yamada, Y. (2011). "Effect of particle size ratio and volume fraction on shear strength of binary granular mixture." *Granular Matter*, 13(6), 731–742.

Valdes, J. R., and Santamarina, J. C. (2006). "Particle clogging in radial flow: Microscale mechanisms." *SPE J.*, 11(02), 193–198.

Valdes, J. R., and Santamarina, J. C. (2008). "Clogging: Bridge formation and vibration-based destabilization." *Can. Geotech. J.*, 45(2), 177–184.

Vallejo, L. E. (2001). "Interpretation of the limits in shear strength in binary granular mixtures." *Can. Geotech. J.*, 38(5), 1097–1104.

Vallejo, L. E., and Lobo-Guerrero, S. (2005). "The elastic moduli of clays with dispersed oversized particles." *Eng. Geol.*, 78(1), 163–171.

Vallejo, L. E., and Mawby, R. (2000). "Porosity influence on the shear strength of granular material-clay mixtures." *Eng. Geol.*, 58(2), 125–136.

Vasil'eva, A. A., Mikheev, V. V., and Lobanova, G. L. (1971). "How the strength properties of gravel soils depend on the type and state of the sand filling the pores." *Soil Mech. Found. Eng.*, 8(3), 167–171.

Vukovic, M., and Soro, A. (1992). *Determination of hydraulic conductivity of porous media from grain-size composition*, Water Resources Publications, Littleton, CO.

Wagg, T. B., and Konrad, J. M. (1990). "Index properties of clay–silt mixtures." *43rd Canadian Geotechnical Conf.*, BiTech Publishers Ltd., Richmond, VA, 705–710.

Watabe, Y., Yamada, K., and Saitoh, K. (2011). "Hydraulic conductivity and compressibility of mixtures of Nagoya clay with sand or bentonite." *Géotechnique*, 61(3), 211–219.

Yamamuro, J. A., and Covert, K. M. (2001). "Monotonic and cyclic liquefaction of very loose sands with high silt content." *J. Geotech. Geoenviron. Eng.*, 10.1061/(ASCE)1090-0241(2001)127:4(314), 314–324.

Yang, S. (2004). "Characterization of the properties of sand–silt mixtures." Ph.D. thesis, Norwegian Univ. of Science and Technology, Trondheim, Norway.

Youd, T. L. (1973). "Factors controlling maximum and minimum densities of sands." *Evaluation of relative density and its role in geotechnical projects involving cohesionless soils*, E. Selig and R. Ladd, eds., ASTM, West Conshohocken, PA, 98–112.

Zhang, Z. F., and Ward, A. L. (2011). "Determining the porosity and saturated hydraulic conductivity of binary mixtures." *Vadose Zone J.*, 10(1), 313–321.

Zlatović, S., and Ishihara, K. (1995). "On the influence of nonplastic fines on residual strength." *Proc., 1st Int. Conf. on Earthquake Geotechnical Engineering (IS-TOKYO '95)*, K. Ishihara, ed., A.A. Balkema, Rotterdam, Netherlands, 239–244.